Graphical Abstract

A Type 2 Wavelet Brain Emotional Learning Network with Double Recurrent Loops based Controller for Nonlinear Systems

Zi-Qi Wang,Li-Jiang Li,Fei Chao,Chih-Min Lin,Longzhi Yang,Changle Zhou,Xiang Chang,Changjing Shang,Qiang Shen

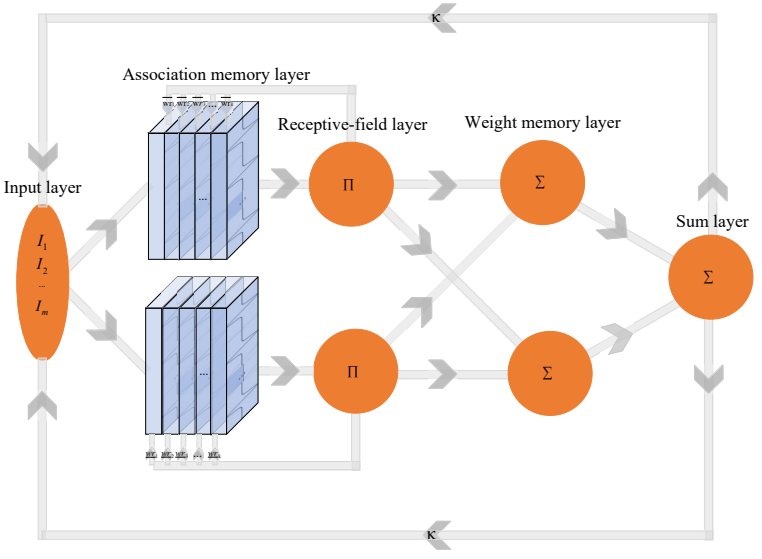

Highlights

A Type 2 Wavelet Brain Emotional Learning Network with Double Recurrent Loops based Controller for Nonlinear Systems

Zi-Qi Wang,Li-Jiang Li,Fei Chao,Chih-Min Lin,Longzhi Yang,Changle Zhou,Xiang Chang,Changjing Shang,Qiang Shen

- Integrating a type-2 wavelet function to a brain emotional network to improve the nonlinear function learning performance.
- Introducing a double-loop structure to a brain emotional network to improve the ability of historical information extraction from dynamic systems.

A Type 2 Wavelet Brain Emotional Learning Network with Double Recurrent Loops based Controller for Nonlinear Systems⋆

Zi-Qi Wang[a], Li-Jiang Li[a], Fei Chao[a,b,*], Chih-Min Lin[c], Longzhi Yang[d], Changle Zhou[a], Xiang Chang[b], Changjing Shang[b] and Qiang Shen[b]

[a]Department of Artificial Intelligence, School of Informatics, Xiamen University, 361005 China
[b]Department of Computer Science, Institute of Mathematics, Physics and Computer Science, Aberystwyth University, SY23 3DB, UK
[c]Department of Electrical Engineering, Yuan Ze University, Taiwan
[d]Department of Computer and Information Sciences, Northumbria University, UK

ARTICLE INFO

Keywords:
Brain emotional learning network
neural network control systems
nonlinear systems
double recurrent neural loops

ABSTRACT

Conventional controllers for nonlinear systems often suffer from co-existences of non-linearity and uncertainty. This paper proposes a novel brain emotional neural network to address such challenges. The proposed network integrates a Type 2 wavelet neural network into a conventional brain emotional learning network which is further enhanced by the introduction of a recurrent structure. The proposed network, therefore, combines the advantages of the Type 2 wavelet function, recurrent mechanism, and brain emotional learning system, so as to obtain optimal performance under uncertain environments. The proposed network works with a compensator to mimic an ideal controller, and the parameters of both the network and compensator are updated based on laws derived from the Lyapunov stability analysis theory. The proposed system was applied to a z-axis microelectromechanical system gyroscope. The experimental results demonstrate that the proposed system outperformed other popular neural-network-based control systems, indicating the superiority of the proposed network-based controller.

1. Introduction

Dynamic control systems such as robots have received extensive attention in recent years [2, 3, 15, 22, 27, 29, 30, 32]. Traditional control methods such as proportional–integral–differential controllers and sliding mode controllers are not very effective for robots to deal with complex and unknown nonlinear systems. However, sliding mode control schemes with embedded neural networks can lead better performances on robots [7, 13, 14, 25, 28]. In addition, self-adaptive control methods can dynamically adjust their parameters according to the characteristics of the controlled systems [9, 12, 18, 31, 35], so as to obtain further enhanced control performance.

Feed-forward neural networks do not acquire and utilize the historical information of dynamic systems. Thus various feedback structures have been integrated into recurrent neural networks for obtaining the historical information of a system under operation, in an effort to allow adaptive parameter adjustment of the control systems [4, 8, 24]. The traditional single feedback structure, such as [5, 8], takes the external signals into consideration, but it does not consider the internal signals. This has led to the development of a double loop recurrent neural network for the control of nonlinear systems with the improved ability of obtaining dynamic information [11]. Such a double loop structure effectively handles both external and internal signals [10, 11], using Gaussian functions as the membership functions. However, these studies did not consider complicated uncertainties and unexpected noises. In contrast, we notice that brain emotional learning neural networks with better nonlinear approximate capabilities has been used in many neural controllers [6, 20]; in addition, the type-2 wavelet structure has been used widely in recent investigations [1, 17, 19, 23, 26], such as the integration of a type-2 wavelet structure into a CMAC network [21]. Inspired by this, this paper introduces the type-2 wavelet as the membership function for better uncertainly handling.

This paper reports a new neural network structure, i.e. a double loop Type-2 wavelet brain emotional learning recurrent neural network (T2WBD), by addressing the key challenge of learning ability in the dynamic system control, so as to make the controller converge to nonlinear function efficiently. In the proposed network, input signals are first fed into the upper and lower channels of a Type-2 wavelet fuzzy structure and then relayed to the sensory and emotional

⋆This work was supported by the Natural Science Foundation of Fujian Province of China (No. 2021J01002).
*Corresponding author
ORCID(s):

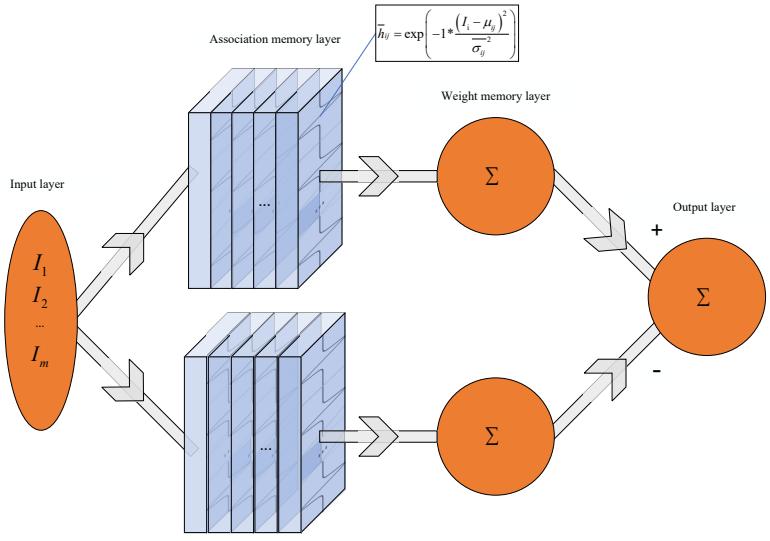

Figure 1: Schematic Diagram of FBEL Structure

channels of a fuzzy brain emotional neural network. The final output of the neural network is an aggregation of the output values of the two channels. In addition, two recurrent loops are created inside the network to improve the ability to acquire dynamic information of unknown controlled objects. The contributions of this paper are summarized as follows: 1) integrating a type-2 wavelet neural network to a brain emotional network for enhanced nonlinear function learning ability under uncertain environments with unexpected noise, and 2) introducing a double looped structure to a brain emotional network for improving the ability of historical information extraction and utilization in dynamic systems.

This remainder of this paper is organized as follows: Section 2 introduces the underpinning of brain emotional learning network; Section 3 presents the proposed network; Section 4 introduces a class of dynamic systems using mathematical expressions, and the structure of the proposed network-based controller; Section 5 specifies comparative experiments and ablation experiments on a z-axis microelectromechanical system gyroscope with experimental results analysis, and Section 6 concludes the work and points out important future work.

2. Background and Related Work

A brain emotional learning neural network (BEL) imitating judgments and emotions of a human brain, consists of two channels, each of which is implemented by a network. Thus, the two networks work independently in the association memory layer and weight memory layer, which then jointly produce the final outputs. In addition, a fuzzy brain emotional learning neural network (FBEL) involving an extra fuzzy inference layer is widely applied in many network-based controllers.

The FBEL network as shown in Fig. 1 consists of the following four layers:

1) Input Layer: Each element in this layer receives one input signal and the input layer is defined as:

$$i = \{i_1, i_2, \ \dots \ , i_m\} \in R^m, \tag{1}$$

where i is a signal and m is the length of i.

2) Association Memory Layer: The output of the input layer is passed to the upper and lower channels. The outputs of these two channels are respectively denoted as f and h:

$$f = \{f_{11}, f_{12}, \dots, f_{1n}, f_{21}, f_{22}, \dots, f_{2n}, \cdots, f_{m1}, f_{m2}, \dots, f_{mn}, \} \in R^{mn}, \tag{2}$$

$$h = \{h_{11}, h_{12}, \dots, h_{1n}, h_{21}, h_{22}, \dots, h_{2n}, \dots, h_{m1}, h_{m2}, \dots, h_{mn}, \} \in R^{mn}, \tag{3}$$

where f and h are two vectors; m is the dimension of the input vector; n is the number of fuzzy rules corresponding to each element of the input vector. In other words, in the lower and upper channel, each element of the input corresponds to a vector, which represents n fuzzy rules. Each element f_{ij} representing the i-th input through the j-th fuzzy rule, thus f_{ij} is defined as:

$$f_{ij} = \exp\left(\frac{-\left(I_i-\mu_{ij}\right)^2}{{\sigma_{ij}}^2}\right) \quad i = 1, 2, \ldots, m; j = 1, 2, \ldots, n \tag{4}$$

where I_i is the i-th input of the system; μ_{ij} represents the center of the Gaussian function, σ_{ij} indicates the width of the Gaussian function f_{ij}. Each element h_{ij}, representing the i-th input through the j-th fuzzy rule, thus h_{ij} is defined as:

$$h_{ij} = \exp\left(\frac{-\left(I_i-b_{ij}\right)^2}{{c_{ij}}^2}\right) \quad i = 1, 2, \ldots, m; j = 1, 2, \ldots, n \tag{5}$$

where b_{ij} represents the center of the Gaussian function, c_{ij} indicates the width of the Gaussian function h_{ij};.

3) Weight Memory Layer: The output of the upper channel, denoted as o, is expressed as:

$$o = \sum_i \sum_j f_{ij} * w_{ij} \quad i = 1, 2, \ldots, m; j = 1, 2, \ldots, n \tag{6}$$

where w_{ij} is the weight of the upper channels corresponding to the output of the i-th line and j-th block in the upper hidden layer of the sensory channel. Similarly, the output of the lower channel, denoted as a, is defined as:

$$a = \sum_i \sum_j h_{ij} * v_{ij} \quad i = 1, 2, \ldots, m; j = 1, 2, \ldots, n \tag{7}$$

where v_{ij} is the weight of the lower channels corresponding to the output of the i-th line and j-th block in the lower hidden layer of the sensory channel.

4) Output Layer:

$$u_{FBELC} = o - a = \sum_i \sum_j f_{ij} * w_{ij} - \sum_i \sum_j h_{ij} * v_{ij} \quad i = 1, 2, \ldots, m; j = 1, 2, \ldots, n \tag{8}$$

where w_{ij} denotes a weight in the sensory channel, and v_{ij} denotes a weight corresponding to the emotional channel. The difference between the outputs of the two channels makes the final output of the network. The updating rules of w and v are defined as:

$$\begin{cases} w_{ij} = w_{ij} + \Delta w_{ij} \\ v_{ij} = v_{ij} + \Delta v_{ij} \end{cases} \tag{9}$$

To be specific, Δw_{ij} and Δv_{ij} are defined by:

$$\begin{cases} \Delta w_{ij} = \beta \times \left[f_{ij} \times \left(u_{\text{FBELC}} - d_i\right)\right] \\ \Delta v_{ij} = \alpha \left[h_{ij} \times \left(\max\left[0, d_i - o\right]\right)\right] \end{cases} \tag{10}$$

where α and β are the learning rates;

The d_i in Eq. 10 is an adjustable parameter that is defined by:

$$d_i = p_i \times I_i + q \times u_{\text{FBELC}} \tag{11}$$

where p and q are the given weight parameters.

3. Proposed Network Structure

The structure of the proposed Type 2 wavelet brain emotional learning network with double recurrent loops is shown in Fig. 2. The network is comprised of an input layer, a hidden layer with feedback, and an output layer. The hidden layer is divided into an upper channel and a lower channel. Each channel contains an association memory layer and a receptive-field layer. The output of the receptive field layer is multiplied by a feedback coefficient and added to the input of the associative memory layer. The output layer aggregates the outputs of the upper and lower channels

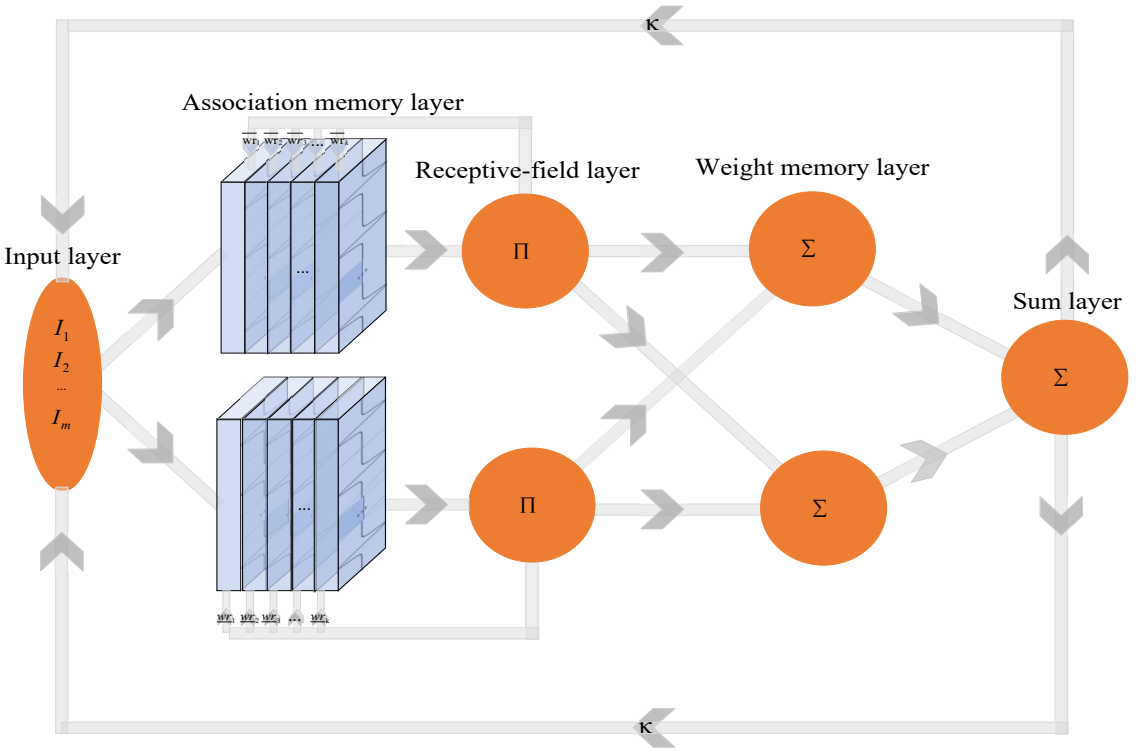

Figure 2: Schematic diagram of T2WBD structure. The channels with κ are the outloop feedback; the channels with γ_i are the internal feedbacks.

to produce the final output of the network. The final output of the neural network and the previous output also act as sources of feedback used by the input of the neural network.

The structure and signal propagation of the proposed network are specified as follows:

1) Input layer: The input of this layer x_i is composed of the external input and historical output of the neural network multiplied by a certain feedback coefficient matrix κ. The output of each neuron node in this layer is expressed as:

$$\begin{cases} I_i = x_i \cdot \gamma_i \\ \gamma = \kappa \cdot R \\ R_j = \dfrac{exnn_j}{eexnn_j} \end{cases} \quad i = 1, 2, 3, \ldots, m; j = 1, 2, 3, \ldots, n \tag{12}$$

where $I = \{i_1, i_2, \ldots, i_i, \ldots, i_m\} \in \Re^m$ is the output signal of the input layer; $x = \left[x_1, x_2, \ldots, x_i, \ldots, x_m\right] \in \Re^m$ is the external input; γ_i is the feedback from the historical output of the neural network; κ is the feedback coefficient matrix of size $m \times n$; n is the number of output nodes of the neural network; m is the number of input nodes of the neural network; $exnn_j$ is last output; $eexnn_j$ is the output prior to $exnn_j$.

2) Association Memory layer: The input signal activates different rows by the associative memory layer. Each row contains several blocks. In each block, the input signal is calculated by the corresponding fuzzy rules, and the generated corresponding output is transmitted to the receptive field layer. Therefore, the outputs of this layer are defined as:

$$\begin{cases} \bar{h}_{ij} = -1 \cdot \dfrac{I_i + \overline{wr}_j \overline{exF}_j - \mu_{ij}}{\bar{\sigma}_{ij}} \cdot \exp\left(-1 \cdot \dfrac{\left(I_i + \overline{wr}_j \overline{exF}_j - \mu_{ij}\right)^2}{\bar{\sigma}_{ij}^{\,2}}\right) \\ \underline{h}_{ij} = -1 \cdot \dfrac{I_i + \underline{wr}_j \underline{exF}_j - \mu_{ij}}{\underline{\sigma}_{ij}} \cdot \exp\left(-1 \cdot \dfrac{\left(I_i + \underline{wr}_j \underline{exF}_j - \mu_{ij}\right)^2}{\underline{\sigma}_{ij}^2}\right) \end{cases} \quad i = 1, 2, 3, \ldots m; j = 1, 2, 3, \ldots, k \tag{13}$$

where $\bar{H} = \left\{\bar{h}_{11}, \bar{h}_{12}, \ldots, \bar{h}_{1k}, \bar{h}_{21}, \bar{h}_{22}, \ldots, \bar{h}_{2k}, \ldots, \bar{h}_{m1}, \bar{h}_{m2}, \ldots, \bar{h}_{mk}\right\} \in R^{mk}$ is the output of the associative memory layer in the upper channel; $\underline{H} = \left\{\underline{h}_{11}, \underline{h}_{12}, \ldots, \underline{h}_{1k}, \underline{h}_{21}, \underline{h}_{22}, \ldots, \underline{h}_{2k}, \underline{h}_{m1}, \underline{h}_{m2}, \ldots, \underline{h}_{mk}\right\} \in R^{mk}$ is the output of

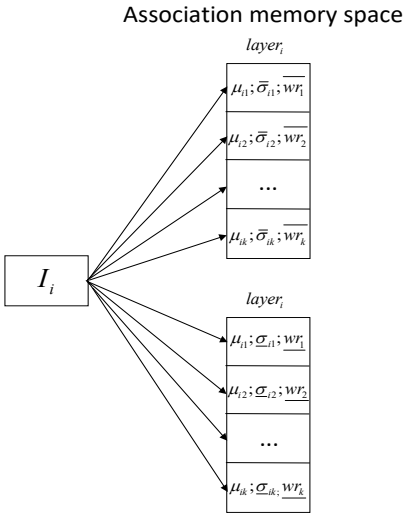

Figure 3: Relationship between input and activation modules

the associative memory layer in the lower channel; m is the dimension of the input vector for the associative memory layer; and k is the number of blocks in each row of the Association Memory layer.

The corresponding relationship between the input and activation modules, as shown in Fig. 3, illustrates that the i-th input value activates each block of the i-th row in the associative memory layer. In addition, $\overline{wr}_j$ and $\underline{wr}_j$ are the weights of internal feedback; $\overline{exF}_j$ and $\underline{exF}_j$ are the outputs of receptive-field; μ_{ij} is the center of the wavelet function; and $\overline{\sigma}_{ij}$ and $\underline{\sigma}_{ij}$ denote the boundaries of a wavelet function.

3) Receptive-Field layer: The output of the associative memory layer is sent to the receptive field layer, and the receptive field is defined as:

$$\begin{cases} \underline{F}_j = \prod_{i=1}^{m} \underline{h}_{ij} \\ \bar{F}_j = \prod_{i=1}^{m} \bar{h}_{ij} \end{cases} \tag{14}$$

where $\bar{F} = \{\bar{F}_1, \bar{F}_2, \cdots, \bar{F}_i, \cdots, \bar{F}_k\} \in R^k$ and $\underline{F} = \{\underline{F}_1, \underline{F}_2, \ldots, \underline{F}_i, \ldots, \underline{F}_k\} \in R^k$ are the outputs of the receptive-field layer; k is the size of the output of the receptive-field layer; $\bar{h}_{ij}$ and $\underline{h}_{ij}$ are the outputs of the association memory layer of the i-th line in the j-th block.

4) Weight memory layer: This layer consists of two neural network channels, which are the sensory neural network channel and emotional neural network channel. The output from the upper channel enters the two channels. The result of the upper channel a is achieved by calculating the difference between the output from the emotional neural network channel and that from the sensory neural network channel:

$$a = \bar{w}\bar{F} - \underline{w}\bar{F}, \tag{15}$$

where $\bar{w} \in R^{n\times k}$ is the amygdala memory weight; $\underline{w} \in R^{n\times k}$ is the prefrontal memory weight; $nn \in R^n$ is the final output.

Similarly, the output from the lower channel also enters two channels, and the output of the lower channel o is similarly generated by subtracting the output of the emotional neural network channel from the output of the sensory neural network channel:

$$o = \bar{w}\underline{F} - \underline{w}\,\underline{F}. \tag{16}$$

5) Sum layer: The final output of the network is generated as the summation of the outputs of the upper and lower

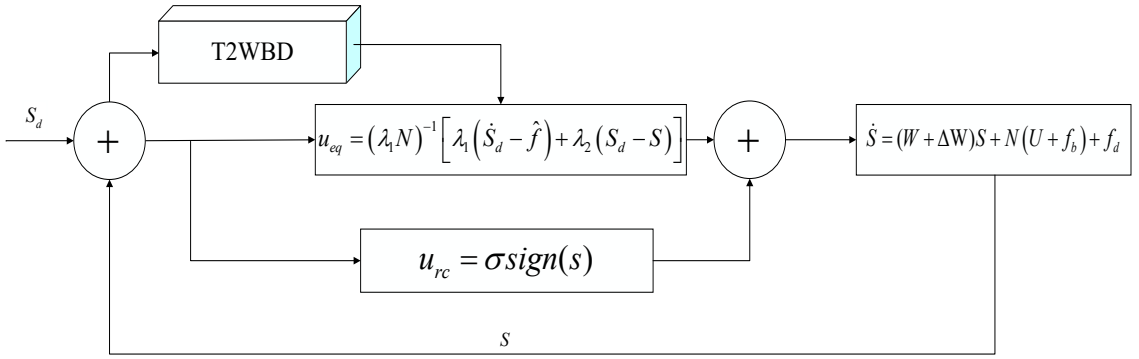

Figure 4: Schematic Diagram of T2WBD Controller Structure. A main controller u_{eq} embedded with T2WBD and a robust controller u_{rc} work together to produce control signals.

channels:

$$nn = a + o. \tag{17}$$

4. Neural Network Controller

4.1. Control Problem Description

The structure of the sliding mode controller is shown in Fig. 4. The controlled object model is a class of nonlinear systems, which can be expressed as:

$$\dot{X} = (W + \Delta W)X + N\left(U + f_b\right) + f_d, \tag{18}$$

where $X \in \Re^m$ is a matrix of variables, including the displacement and speed of the control system representing the state of the system; $W \in \Re^{m\times m}$ and $N \in \Re^{m\times q}$ are constant matrices, which are important parameters constituting the system; $U \in \Re^q$ is a variable matrix, representing the complete control value for the system; ΔW represents the uncertainty of W; $f_b \in \Re^q$ is a non-linear function; f_d is an external disturbance. Thus, the nominal model of this class of systems is defined as:

$$\dot{X} = WX + NU + F, \tag{19}$$

where F is a lumped formula of parameter uncertainty and external interference, which is defined by:

$$F = \Delta WX + Nf_b + f_d. \tag{20}$$

Assuming that the lumped equation F is bounded, then we have $\mid F \mid \leq F_d$, where F_d is a positive constant. Given the nonlinear system model as expressed above, the control task is to find a controller so that the tracking trajectory X can track the reference trajectory X_d. Therefore, the error between the tracking trajectory and the reference trajectory is defined as: $e = X_d - X$, and the derivative of the error is: $\dot{e} = \dot{X}_d - \dot{X}$. The sliding mode surface, s, of the system is a linear combination of the error and the derivative of the error; s is then defined as:

$$s = \begin{bmatrix} \lambda_{11} & \dots & 0 & \dots & \lambda_{n1} & \dots & 0 \\ & \ddots & & \dots & & \ddots & \\ 0 & \dots & \lambda_{1m} & \dots & 0 & \dots & \lambda_{nm} \end{bmatrix} \begin{bmatrix} \underline{e} \\ \int_0^T edt \end{bmatrix} \tag{21}$$

where $\underline{e}^{\mathrm{T}} = \{e^{(n-1)}, ..., \dot{e}, e\}$ is a column vector, which consists of the tracking error e and its derivative. The coefficient matrix on the left side can be simplified as:

$$\lambda = \begin{bmatrix} \lambda_{11} & \dots & 0 & \dots & \lambda_{n1} & \dots & 0 \\ & \ddots & & \dots & & \ddots & \\ 0 & \dots & \lambda_{1m} & \dots & 0 & \dots & \lambda_{rn} \end{bmatrix} = \left[\lambda_1, \lambda_2\right] \tag{22}$$

Eq. 21 is simplified to:

$$s = \lambda_1 e + \lambda_2 \int e. \tag{23}$$

Differentiate Eq. 23 with respect to time:

$$\dot{s} = \lambda_1 \left(\dot{X}_d - \dot{X}\right) + \lambda_2 \left(X_d - X\right). \tag{24}$$

Substitute Eq. 19 into Eq. 24, the following can be obtained:

$$\dot{s} = \lambda_1 \left(\dot{X}_d - WX - NU - F\right) + \lambda_2 \left(X_d - X\right). \tag{25}$$

If the sliding surface is reachable, the following mathematical expression must be satisfied:

$$\frac{1}{2}\frac{d}{dt}\left(s_i^2\right) \leq -\sum_{m}^{i=1} \sigma_i \left|s_i\right|. \tag{26}$$

Substitute Eq. 25 into Eq. 26, yielding:

$$s \cdot \dot{s} = s\left[\lambda_1 \left(\dot{X}_d - WX - NU - F\right) + \lambda_2 \left(X_d - X\right)\right] \leq -\sum_{m}^{i=1} \sigma_i \left|s_i\right|. \tag{27}$$

Set $\dot{s}$= 0, then the ideal controller U_{eq} is defined as:

$$U_{eq} = \left(\lambda_1 N\right)^{-1}\left[\lambda_1 \left(\dot{X}_d - WX\right) + \lambda_2 \left(X_d - X\right) - \lambda_1 F\right]. \tag{28}$$

Based on Eq. 28, the neural network controller is defined as:

$$U = \left(\lambda_1 N\right)^{-1}\left[\lambda_1 \left(\dot{X}_d - WX\right) + \lambda_2 \left(X_d - X\right) - U_{rc}\right]. \tag{29}$$

where $U_{rc} = \sigma sgn(s)$.Then, the Lyapunov function of the control system is defined as:

$$V = \frac{1}{2} s^T s. \tag{30}$$

Differentiate Eq. 30 with respect to time, then substitute Eq. 25 into the derivative of the Eq. 30 leading to:

$$\dot{V} = s^T \dot{s} = s^T \left[\lambda_1 \left(\dot{X}_d - WX - NU - F\right) + \lambda_2 \left(X_d - X\right)\right]. \tag{31}$$

Substitute Eq. 29 into Eq. 31, we have:

$$\begin{aligned} \dot{V} &= s^T \left(-\sigma sgn(s) - \lambda_1 F\right) \\ &= -\sigma|s| - s^T \lambda_1 F \leq -\sigma|s| + \lambda_1 F_d |s| \\ &= -|s|\left(\sigma - \lambda_1 F_d\right). \end{aligned} \tag{32}$$

Set $\sigma > \lambda_1 F_d$, then $\dot{V} < 0$. According to Barbalat's lemma, s will gradually converge to 0; this means, based on Eq. 24, e will gradually converge to 0. However, the parameter matrix, W as defined in Eq. 28, in the ideal sliding mode controller is unknown. The next section introduces how to use the proposed neural network to solve this problem.

4.2. Rule Update

This paper uses the proposed neural network, T2WBD, to approximate W and X, then the model expressed in Eq. 19 can be rewritten as:

$$\dot{X} = f + NU + F. \tag{33}$$

Assuming that a set of ideal parameters, $\bar{w}^*$, $\underline{w}^*$, wr^*, κ^*, μ^*, σ^*, exist. Therefore, we have:

$$f^* = \bar{w}^* \bar{F}^* - \underline{w}^* \bar{F}^* + (\bar{w}^* \underline{F}^* - \underline{w}^* \underline{F}^*) \tag{34}$$

Based on Eq. 25, the neural network controller is defined as:

$$U = \left(\lambda_1 N\right)^{-1} \left[\lambda_1 \left(\dot{X}_d - WX\right) + \lambda_2 \left(X_d - X\right) - \lambda_1 F - \dot{s}\right]. \tag{35}$$

Accordingly to Eqs. 29 and 35, $\dot{s}$ is defined as:

$$\dot{s} = \left(\lambda_1\right) \left(-\hat{W}\hat{X} + W^* X^*\right) - \lambda_1 F - U_{rc}. \tag{36}$$

Thus Eq. 36 can be rewritten as:

$$\dot{s} = \left(\lambda_1\right) \left(-\hat{f} + f^*\right) - \lambda_1 F - U_{rc}). \tag{37}$$

The lower channel is updated using an emotional learning rate. Therefore, this paper only considers the upper channel, then the approximation error is:

$$\begin{aligned} f^* - \hat{f} &= \bar{w}^*(\bar{F}^* + \underline{F}^*) - \hat{\bar{w}}(\hat{\bar{F}} + \hat{\underline{F}}) + \varepsilon \\ &= (\hat{\bar{w}} + \tilde{\bar{w}}) * (\hat{\bar{F}} + \tilde{\bar{F}} + \hat{\underline{F}} + \tilde{\underline{F}}) - \hat{\bar{w}}(\hat{\bar{F}} + \hat{\underline{F}}) + \varepsilon \\ &= \hat{\bar{w}}\tilde{\bar{F}} + \tilde{\bar{w}}\hat{\bar{F}} + \tilde{\bar{w}}\tilde{\bar{F}} + \hat{\bar{w}}\tilde{\underline{F}} + \tilde{\bar{w}}\hat{\underline{F}} + \hat{\bar{w}}\tilde{\underline{F}} + \varepsilon \end{aligned} \tag{38}$$

where ε is an approximation error.

Using the Taylor expansion to respectively transform $\tilde{\bar{F}}$ and $\tilde{\underline{F}}$ in Eq. 38, the following can be generated:

$$\begin{aligned} \tilde{\bar{F}} &= \left.\frac{\partial \tilde{\bar{F}}}{\partial \mu}\right|_{\mu=\hat{\mu}} \left(\mu^* - \hat{\mu}\right) + \left.\frac{\partial \tilde{\bar{F}}}{\partial \bar{\sigma}}\right|_{\bar{\sigma}=\hat{\bar{\sigma}}} \left(\bar{\sigma}^* - \hat{\bar{\sigma}}\right) \\ &+ \left.\frac{\partial \tilde{\bar{F}}}{\partial wr}\right|_{\bar{w}r=\hat{\bar{w}}r} \left(\bar{w}r^* - \hat{\bar{w}}r\right) + \left.\frac{\partial \tilde{\bar{F}}}{\partial \kappa}\right|_{\kappa=\hat{\kappa}} \left(\kappa^* - \hat{\kappa}\right) + \Delta_1 \\ &= D\overline{F}_{\mu} \cdot \tilde{\mu} + D\overline{F}_{\bar{\sigma}} \cdot \tilde{\bar{\sigma}} + D\overline{F}_{\bar{w}r} \cdot \tilde{\bar{w}}r + D\overline{F}_{\kappa} \cdot \tilde{\kappa} + \Delta_1, \end{aligned} \tag{39}$$

$$\begin{aligned} \tilde{\underline{F}} &= \left.\frac{\partial \tilde{\underline{F}}}{\partial \mu}\right|_{\mu=\hat{\mu}} \left(\mu^* - \hat{\mu}\right) + \left.\frac{\partial \tilde{\underline{F}}}{\partial \underline{\sigma}}\right|_{\underline{\sigma}=\hat{\underline{\sigma}}} \left(\underline{\sigma}^* - \hat{\underline{\sigma}}\right) \\ &+ \left.\frac{\partial \tilde{\underline{E}}}{\partial wr}\right|_{\underline{wr}=\hat{\underline{w}}r} \left(\underline{wr}^* - \hat{\underline{w}}r\right) + \left.\frac{\partial \tilde{\underline{F}}}{\partial \kappa}\right|_{\kappa=\hat{\kappa}} \left(\kappa^* - \hat{\kappa}\right) + \Delta_2 \\ &= D\underline{F}_{\mu} \cdot \tilde{\mu} + D\underline{F}_{\underline{\sigma}} \cdot \tilde{\underline{\sigma}} + D\underline{F}_{\underline{wr}} \cdot \tilde{\underline{w}}r + D\underline{F}_{\kappa} \cdot \tilde{\kappa} + \Delta_2, \end{aligned} \tag{40}$$

where Δ_1 and Δ_2 are combinations of higher order terms. $\tilde{\mu}$, $\tilde{\bar{\sigma}}$, $\tilde{\bar{w}}r$, $\tilde{\kappa}$, $\tilde{\sigma}$ and $\tilde{\underline{w}}r$ are respectively defined as:

$$\tilde{\mu} = \left\{\tilde{\mu}_{11}\tilde{\mu}_{12} \cdots \tilde{\mu}_{1k} \cdots \tilde{\mu}_{mk}\right\} \tag{41}$$

$$\tilde{\bar{\sigma}} = \left\{\tilde{\bar{\sigma}}_{11}\tilde{\bar{\sigma}}_{12} \cdots \tilde{\bar{\sigma}}_{1k} \cdots \tilde{\bar{\sigma}}_{mk}\right\} \tag{42}$$

$$\tilde{\sigma} = \left\{\tilde{\underline{\sigma}}_{11}\tilde{\underline{\sigma}}_{12} \cdots \tilde{\underline{\sigma}}_{1k} \cdots \tilde{\underline{\sigma}}_{mk}\right\} \tag{43}$$

$$\tilde{\bar{w}}r = \left\{\tilde{\bar{w}}r_1\tilde{\bar{w}}r_2 \ldots \tilde{\bar{w}}r_k\right\} \tag{44}$$

$$\tilde{\underline{w}}r = \left\{\tilde{\underline{w}}r_1\tilde{\underline{w}}r_2 \ldots \tilde{\underline{w}}r_k\right\} \tag{45}$$

$$\tilde{\kappa} = \left\{\tilde{\kappa}_{11}\tilde{\kappa}_{12} \ldots \tilde{\kappa}_{1n} \ldots \tilde{\kappa}_{mn}\right\}. \tag{46}$$

Thus, $D\overline{F}_{\mu}$, $D\overline{F}_{\bar{\sigma}}$, $D\overline{F}_{\bar{w}r}$, $D\overline{F}_{\kappa}$, $D\underline{F}_{\mu}$, $D\underline{F}_{\underline{\sigma}}$, $D\underline{F}_{\underline{wr}}$ and $D\underline{F}_{\underline{\kappa}}$ are respectively defined as:

$$D\bar{F}_{\bar{\sigma}} = \begin{bmatrix} \begin{bmatrix} \overbrace{\frac{\partial \tilde{\bar{F}}_1}{\partial \bar{\sigma}_{11}} \cdots \frac{\partial \tilde{\bar{F}}_1}{\partial \bar{\sigma}_{m1}}}^{m} \overbrace{0 \ldots 0}^{m(k-1)} \end{bmatrix} \\ \cdots \\ \begin{bmatrix} \overbrace{0 \ldots 0}^{m(i-1)} \overbrace{\frac{\partial \tilde{\bar{F}}_i}{\partial \bar{\sigma}_{1i}} \cdots \frac{\partial \tilde{\bar{F}}_i}{\partial \bar{\sigma}_{mi}}}^{m} \overbrace{0 \ldots 0}^{m(k-i)} \end{bmatrix} \\ \cdots \\ \begin{bmatrix} \overbrace{0 \ldots 0}^{m(k-1)} \overbrace{\frac{\partial \tilde{\bar{F}}_k}{\partial \bar{\sigma}_{1k}} \cdots \frac{\partial \tilde{\bar{F}}_k}{\partial \bar{\sigma}_{mk}}}^{m} \end{bmatrix} \end{bmatrix} \tag{47}$$

$$D\bar{F}_{\bar{w}r} = \begin{bmatrix} \begin{bmatrix} \frac{\partial \tilde{\bar{F}}_1}{\partial \bar{wr}_1} \overbrace{0 \ldots 0}^{k-1} \end{bmatrix} \\ \cdots \\ \begin{bmatrix} \overbrace{0 \ldots 0}^{i-1} \frac{\partial \tilde{\bar{F}}_i}{\partial \bar{wr}_i} \overbrace{0 \ldots 0}^{k-i} \end{bmatrix} \\ \cdots \\ \begin{bmatrix} \overbrace{0 \ldots 0}^{k-1} \frac{\partial \tilde{\bar{F}}_k}{\partial \bar{wr}_k} \end{bmatrix} \end{bmatrix} \tag{48}$$

$$D\bar{F}_{\kappa} = \begin{bmatrix} \begin{bmatrix} \frac{\partial \bar{\tilde{F}}_1}{\partial \kappa_{11}} \cdots \frac{\partial \bar{\tilde{F}}_1}{\partial \kappa_{m1}} \\ \frac{\partial \bar{\tilde{F}}_2}{\partial \kappa_{11}} \cdots \frac{\partial \bar{\tilde{F}}_2}{\partial \kappa_{m1}} \\ \cdots \\ \frac{\partial \bar{\tilde{F}}_k}{\partial \kappa_{11}} \cdots \frac{\partial \bar{\tilde{F}}_k}{\partial \kappa_{m1}} \end{bmatrix} \\ \cdots \\ \begin{bmatrix} \frac{\partial \bar{\tilde{F}}_1}{\partial \kappa_{1i}} \cdots \frac{\partial \bar{\tilde{F}}_1}{\partial \kappa_{mi}} \\ \frac{\partial \bar{\tilde{F}}_2}{\partial \kappa_{1i}} \cdots \frac{\partial \bar{\tilde{F}}_2}{\partial \kappa_{mi}} \\ \cdots \\ \frac{\partial \bar{\tilde{F}}_k}{\partial \kappa_{1i}} \cdots \frac{\partial \bar{\tilde{F}}_k}{\partial \kappa_{mi}} \end{bmatrix} \\ \cdots \\ \begin{bmatrix} \frac{\partial \bar{\tilde{F}}_1}{\partial \kappa_{1n}} \cdots \frac{\partial \bar{\tilde{F}}_1}{\partial \kappa_{mk}} \\ \frac{\partial \bar{\tilde{F}}_2}{\partial \kappa_{1n}} \cdots \frac{\partial \bar{\tilde{F}}_2}{\partial \kappa_{mk}} \\ \cdots \\ \frac{\partial \bar{\tilde{F}}_k}{\partial \kappa_{1n}} \cdots \frac{\partial \bar{\tilde{F}}_k}{\partial \kappa_{mk}} \end{bmatrix} \end{bmatrix} \tag{49}$$

$$D\underline{F}_{\mu} = \begin{bmatrix} \begin{bmatrix} \overbrace{\frac{\partial \tilde{F}_1}{\partial \mu_{11}} \cdots \frac{\partial \tilde{F}_1}{\partial \mu_{m1}}}^{m} \overbrace{0 \ldots 0}^{m(k-1)} \end{bmatrix} \\ \cdots \\ \begin{bmatrix} \overbrace{0 \ldots 0}^{m(i-1)} \overbrace{\frac{\partial \tilde{F}_i}{\partial \mu_{1i}} \cdots \frac{\partial \tilde{F}_i}{\partial \mu_{mi}}}^{m} \overbrace{0 \ldots 0}^{m(k-i)} \end{bmatrix} \\ \cdots \\ \begin{bmatrix} \overbrace{[0 \ldots 0}^{m(k-i)} \overbrace{\frac{\partial \tilde{F}_k}{\partial_{\mu_{1k}}} \cdots \frac{\partial \tilde{F}_k}{\partial_{\mu_{mk}}}}^{m}] \end{bmatrix} \end{bmatrix} \tag{50}$$

$$D\underline{F}_{\underline{\sigma}} = \begin{bmatrix} \begin{bmatrix} \overbrace{\frac{\partial \tilde{F}_1}{\partial_{\underline{\sigma}_{11}}} \cdot \cdot \frac{\partial \tilde{F}_1}{\partial_{\underline{\sigma}_{m1}}}}^{m} \overbrace{0 \ldots 0}^{m(k-1)} \end{bmatrix} \\ \cdots \\ \begin{bmatrix} \overbrace{0 \ldots 0}^{m(i-1)} \overbrace{\frac{\partial \underline{\tilde{F}}_i}{\partial_{\underline{\sigma}_{1i}}} \cdots \frac{\partial \underline{\tilde{F}}_i}{\partial_{\underline{\sigma}_{mi}}}}^{m} \overbrace{0 \ldots 0}^{m(k-i)} \end{bmatrix} \\ \cdots \\ \begin{bmatrix} \overbrace{0 \ldots 0}^{m(k-i)} \overbrace{\frac{\partial \tilde{F}_k}{\partial_{\sigma_{1k}}} \cdots \frac{\partial \tilde{F}_k}{\partial_{\sigma_{mk}}}}^{m} \end{bmatrix} \end{bmatrix} \tag{51}$$

$$D\underline{F}_{\underline{w}r} = \begin{bmatrix} \left[\frac{\partial \underline{\tilde{F}}_1}{\partial \bar{w}r_1} \overbrace{0 \dots 0}^{k-1} \right] \\ \dots \\ \left[\overbrace{[0 \dots 0}^{i-1} \frac{\partial \underline{\tilde{F}}_i}{\partial \bar{w}r_i} \overbrace{0 \dots 0]}^{k-i} \right] \\ \dots \\ \left[\overbrace{[0 \dots 0}^{k-1} \frac{\partial \underline{\tilde{F}}_k}{\partial \bar{w}r_k}] \right] \end{bmatrix} \tag{52}$$

$$D\underline{F}_{\kappa} = \begin{bmatrix} \begin{bmatrix} \frac{\partial \underline{\tilde{F}}_1}{\partial \kappa_{11}} \dots \frac{\partial \underline{\tilde{F}}_1}{\partial \kappa_{m1}} \\ \frac{\partial \underline{\tilde{F}}_2}{\partial \kappa_{11}} \dots \frac{\partial \underline{\tilde{F}}_2}{\partial \kappa_{m1}} \\ \dots \\ \frac{\partial \underline{\tilde{F}}_k}{\partial \kappa_{11}} \dots \frac{\partial \underline{\tilde{F}}_k}{\partial \kappa_{m1}} \end{bmatrix} \\ \dots \\ \begin{bmatrix} \frac{\partial \underline{\tilde{F}}_1}{\partial \kappa_{1i}} \dots \frac{\partial \underline{\tilde{F}}_1}{\partial \kappa_{mi}} \\ \frac{\partial \underline{\tilde{F}}_2}{\partial \kappa_{1i}} \dots \frac{\partial \underline{\tilde{F}}_2}{\partial \kappa_{mi}} \\ \dots \\ \frac{\partial \underline{\tilde{F}}_k}{\partial \kappa_{1i}} \dots \frac{\partial \underline{\tilde{F}}_k}{\partial \kappa_{mi}} \end{bmatrix} \\ \dots \\ \begin{bmatrix} \frac{\partial \underline{\tilde{F}}_1}{\partial \kappa_{1n}} \dots \frac{\partial \underline{\tilde{F}}_1}{\partial \kappa_{mn}} \\ \frac{\partial \underline{\tilde{F}}_2}{\partial \kappa_{1n}} \dots \frac{\partial \underline{\tilde{F}}_2}{\partial \kappa_{mn}} \\ \dots \\ \frac{\partial \underline{\tilde{F}}_k}{\partial \kappa_{1n}} \dots \frac{\partial \underline{\tilde{F}}_k}{\partial \kappa_{mn}} \end{bmatrix} \end{bmatrix} \tag{53}$$

Substitute Eqs. 39 and 40 into Eq. 38:

$$\begin{aligned} f^* - \hat{f} &= \hat{\tilde{w}}\tilde{\bar{F}} + \tilde{\tilde{w}}\hat{\bar{F}} + \tilde{\tilde{w}}\tilde{\bar{F}} + \hat{\tilde{w}}\underline{\tilde{F}} + \tilde{\tilde{w}}\underline{\hat{F}} + \tilde{\tilde{w}}\underline{\tilde{F}} + \varepsilon \\ &= \hat{\tilde{w}}(D\bar{F}_{\mu} \cdot \tilde{\mu} + D\bar{F}_{\sigma} \cdot \tilde{\bar{\sigma}} + D\bar{F}_{\underline{w}r} \cdot \underline{\tilde{w}r} + D\bar{F}_{\kappa} \cdot \\ &\quad \tilde{\kappa} + \Delta_1) + \tilde{\tilde{w}}\hat{\bar{F}} + \hat{\tilde{w}}(D\underline{F}_{\mu} \cdot \tilde{\mu} + D\underline{F}_{\underline{\sigma}} \cdot \underline{\tilde{\sigma}} + D\underline{F}_{\underline{w}r} \\ &\quad \cdot \underline{\tilde{w}r} + D\underline{F}_{\kappa} \cdot \tilde{\kappa} + \Delta_2) + \tilde{\tilde{w}}\hat{\bar{F}} + \tilde{\tilde{w}}\tilde{\bar{F}} + \tilde{\tilde{w}}\underline{\tilde{F}} + \varepsilon \\ &= \hat{\tilde{w}}(D\bar{F}_{\mu} \cdot \tilde{\mu} + D\bar{F}_{\tilde{\sigma}} \cdot \tilde{\bar{\sigma}} + D\bar{F}_{\bar{w}r} \cdot \tilde{\bar{w}}r + D\bar{F}_{\kappa} \cdot \tilde{\kappa}) \\ &\quad + \tilde{\tilde{w}}\hat{\bar{F}} + \hat{\tilde{w}}(D\underline{F}_{\mu} \cdot \tilde{\mu} + D\underline{F}_{\underline{\sigma}} \cdot \underline{\tilde{\sigma}} + D\underline{F}_{\underline{w}r} \cdot \underline{\tilde{w}r} + D\underline{F}_{\kappa} \\ &\quad \cdot \tilde{\kappa}) + \tilde{\tilde{w}}\underline{\hat{F}} + \tilde{\tilde{w}}\tilde{\bar{F}} + \tilde{\tilde{w}}\underline{\tilde{F}} + \hat{\tilde{w}}\Delta_1 + \hat{\tilde{w}}\Delta_2 + \varepsilon \\ &= \hat{\tilde{w}}(D\bar{F}_{\mu} \cdot \tilde{\mu} + D\bar{F}_{\tilde{\sigma}} \cdot \tilde{\bar{\sigma}} + D\bar{F}_{\tilde{w}r} \cdot \tilde{\bar{w}}r + D\bar{F}_{\kappa} \cdot \tilde{\kappa}) \\ &\quad + \tilde{\tilde{w}}\hat{\bar{F}} + \hat{\tilde{w}}(D\underline{F}_{\underline{\mu}} \cdot \tilde{\mu} + D\underline{F}_{\underline{\sigma}} \cdot \tilde{\sigma} + D\underline{F}_{\underline{w}r} \cdot \underline{\tilde{w}r} + D\underline{F}_{\kappa} \\ &\quad \cdot \tilde{\kappa}) + \underline{\tilde{w}}\hat{\underline{F}} + \tau \end{aligned} \tag{54}$$

where $\tau = \tilde{\tilde{w}}\tilde{\bar{F}} + \tilde{\tilde{w}}\underline{\tilde{F}} + \hat{\tilde{w}}\Delta_1 + \hat{\tilde{w}}\Delta_2 + \varepsilon$ and we assume τ is bounded, that is: $\mid \tau \mid \leq \tau_0$. Then, the Lyapunov function

is used to analyze the asymptotic stability of the control system based on the proposed T2WBD; and the prove process is specified in the appendix section.

5. Simulations

5.1. Simulation Setup

The simulated environment of this experiment is the dynamic model of a gyroscope, which is expressed as:

$$\dot{X} = (W + \Delta W)X + N\left(U + f_b\right) + f_d \tag{55}$$

where X is defined as:

$$X = \begin{bmatrix} x & \dot{x} & y & \dot{y} \end{bmatrix}^T \tag{56}$$

where x and $\dot{x}$ are the displacement and velocity in the x direction; y and $\dot{y}$ are the displacement and velocity in the y direction, respectively. Thus, U in Eq. 55 is defined as:

$$U = \begin{bmatrix} u_x \\ u_y \end{bmatrix} \tag{57}$$

where u_x and u_y are the outputs of the control system. Thus, W and N in Eq. 55 are defined as:

$$W = \begin{bmatrix} 0 & 1 & 0 & 0 \\ -\omega_x^2 & -d_{xx} & -\omega_{xy} & -\left(d_{xy} - 2\Omega_z\right) \\ 0 & 0 & 0 & 1 \\ -\omega_{xy} & -\left(d_{xy} + 2\Omega_z\right) & -\omega_y^2 & -d_{yy} \end{bmatrix} \tag{58}$$

$$N = \begin{bmatrix} 0 & 0 \\ 1 & 0 \\ 0 & 0 \\ 0 & 1 \end{bmatrix} \tag{59}$$

where ΔW represents the uncertainty of W; the changing range of ΔW in this experiment is set to $\Delta W = W * (rand(1) * 0.6 - 0.3)$; and f_b is a non-linear function, which is defined as:

$$f_b = [10\sin(2t) \quad 5\sin(\pi t)\cos(2\pi t)]^T \tag{60}$$

where f_d is a random function that represents external interference, and f_d is defined as:$f_d = [rand(1)\ rand(1)\ rand(1)\ rand(1)]^T$. λ_1 and λ_2 are system parameters, defined by: $\lambda_1 = \begin{bmatrix} 0\,1\,0\,0 \\ 0\,0\,0\,1 \end{bmatrix}$, $\lambda_2 = \begin{bmatrix} 0\,240\,0\,0 \\ 0\,0\,0\,300 \end{bmatrix}$. The weights, means, and variances of the proposed network are initialized with random values.

The parameters in Eqs. (66)-(72) are set as follow: $\eta 1 = 25$, $\eta 3 = 1.5$, $\eta 4 = 2.5$, $\eta 5 = 2.5$, $\eta 6 = 1.2$, $\eta 7 = 1.2$, $\eta 8 = 105$. The learning rate b and gain parameter c in Eqs. (68) and (69) are set to 0.01 and 0.01, respectively.

5.2. Comparative Study

This experiment compared the efficiency of the proposed neural network against three traditional neural networks, including the Fuzzy Brain Emotional Learning Network (FBEL) [20], Fuzzy Cerebellar Model Articulation Controller Network (FCMAC) [16], and Double Loop Recurrent Neural Network DLRNN [11] by simulating trajectory tracking. The objective of the controllers is to effectively track the reference trajectory. The tracking performances of these controllers are reflected by their error converging speed and tracking accuracies. In this simulation, the reference trajectory is a piecewise function, which is defined by:

$$\begin{aligned} x &= \begin{cases} \sin(4.17t) & 0 < t \le 4\pi \\ 1.2\sin(5.11t) & 4\pi < t \le 30 \end{cases} \\ y &= \begin{cases} 1.2\sin(5.11t) & 0 < t \le 4\pi \\ \sin(4.17t) & 4\pi < t \le 30 \end{cases} \end{aligned} \tag{61}$$

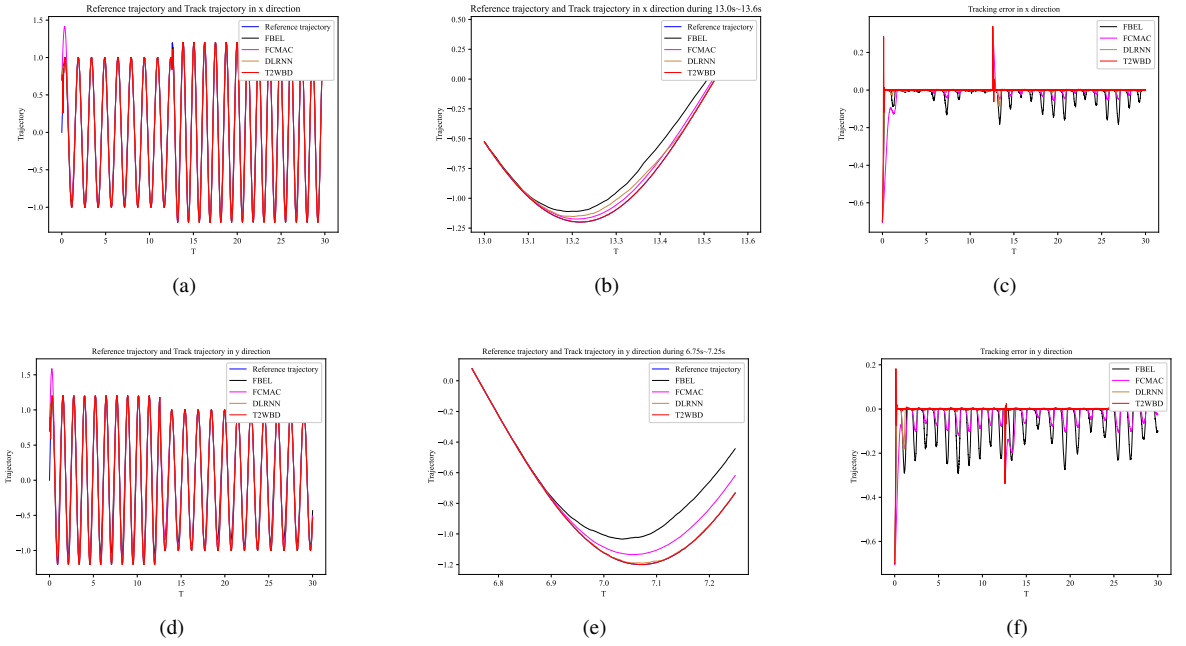

Figure 5: The simulated position responses and tracking errors led by the proposed T2WBD and compared controllers

where t represents the t-th time step. The complete control time is set to 30 seconds. The initial state of the system is set to [0.7 0.1 0.7 0.1].

The tracked trajectory, tracking errors, and their magnified versions in both x-direction and y-direction are shown in Fig. 5. In this figure, lines are colour coded to distinguish the results led by different controllers; in particular, the reference trajectory is represented by a blue line, and the tracking trajectories generated by the FBEL, FCMAC, DLRNN, and proposed T2WBD are shown by the black line, pink line, brown line, and red line, respectively.

The overall tracking performance of the proposed and the compared approaches during the entire control process are illustrated in Figs. 5(a) and 5(d). All the neural network-based controllers successfully followed the reference trajectory after a settling-down term. However, the FBEL and FCMAC based controllers were not very stable during the several peak regions. In contrast, the DLRNN and proposed T2WBD can always closely follow the reference trajectory.

To better distinguish the performance of different controllers after the settling down period, a zoomed in presentation of the tracking in the x direction from 13.0s to 13.6s and in the y direction from 6.75s to 7.25s are shown in Figs. 5(b) and 5(e) respectively. As shown in Fig. 5(b), from 13.1s, all the network-based controllers generated tracking errors in various degrees, but the errors generated by the FBEL-based controller were the most significant amongst all the controllers; the DLRNN and FCMAC based controllers have led to smaller errors than FBEL. In contrast, the errors led by the proposed T2WBD were the smallest within all the competing controllers, which is also confirmed by Fig. 5(e).

Figs. 5(c) and 5(f) demonstrate the overall changing curves of the tracking errors over time. Due to the change of reference trajectory at $4 \times \pi s$, all controllers showed large errors at about $12.6s$. Noticeably, the proposed T2WBD controller demonstrated the fastest converging speed and the smallest errors amongst all employed controllers in this experiment.

The sums of the squared errors and mean square errors of the tracking trajectory led by different neural network controllers in both the x-direction and y-direction are summarized in Tables 1 and 2, respectively. These tables also suggest the proposed T2WBD exhibited better tracking performance than other neural network-based controllers.

Table 1
Comparison of Approximation Performance in the x-direction in the comparative study

Neural Network	(SSE)	(MSE)
FBEL	98.881548	0.000329605
FCMAC	173.935847	0.005797862
DLRNN	49.114993	0.000163717
T2WBD	**37.953864**	**0.000126513**

Table 2
Comparison of Approximation Performance in the y-direction in the comparative study

Neural Network	(SSE)	(MSE)
FBEL	305.128964	0.001017097
FCMAC	202.423319	0.006747444
DLRNN	49.681338	0.000165604
T2WBD	**36.094869**	**0.000120316**

Table 3
Comparison of Approximation Performance in the x-direction in the ablation simulation

Neural Network	(SSE)	(MSE)
T2WBD w/o External	32.160703	0.000107202
T2WBD w/o Internal	76.536125	0.000255120
T2WBD w/o Type 2	44.114399	0.000147048
T2WBD w/o FBEL	46.077371	0.000153591
T2WBD	29.060304	0.000096868

Table 4
Comparison of Approximation Performance in the y-direction in the ablation simulation

Neural Network	(SSE)	(MSE)
T2WBD w/o External	29.137434	0.000097125
T2WBD w/o Internal	75.402097	0.000251340
T2WBD w/o Type 2	40.416374	0.000134721
T2WBD w/o FBEL	64.222966	0.000214077
T2WBD	28.395072	0.000094650

5.3. Ablation Simulation

The second experiment used three ablation simulations to show the effect of the recurrent structure, the Type 2 wavelet function, and the brain emotional structure. The reference trajectories of the second simulation was set to:

$$\begin{cases} \mathrm{x} = \sin(4.17t) \\ y = 1.2 \cdot \sin(5.11t) \end{cases} \tag{62}$$

where t represents time. In this experiment, the whole control time was set to 30 seconds, and the initial state of the system was set to [0.70.10.70.1].

Tables 3 and 4 respectively show the sum of squared errors and the mean square errors in the x-direction and y-direction led by different network setups, including the basic structure (1) without external loop, (2) without internal loop, (3) without Type 2 fuzzification layer, and (4) without FBEL structure. These two tables show that the inner loop, Type 2 layer, and FBEL mechanisms played a key role in the controllers, as the values of both SSE and MSE were increased significantly without the inclusion of these mechanisms. In contrast, the effect of the out loop structure was not as important as those other investigated mechanisms; because both SSE and MSE led by these were close to those of the full structure of T2WBD.

6. Conclusion

This paper reported a new controller which integrates a type-2 wavelet function to a brain emotional network for enhanced nonlinear function learning ability with the support of a double-loop structure to the emotional network for effective use of historical information of dynamic systems. The stability of the controller is guaranteed by an adaptive learning approach, which is developed based on the Lyapunov theory. The proposed network was embedded in a network-based controller structure targeting a class of nonlinear systems. The controller was composed of a neural network and a robust controller, to realize efficient tracking performance of nonlinear systems. The control strategy proposed in this paper was applied to a z-axis MEMS gyroscope. Through comparative study and ablation simulations, it is proved that the proposed neural network structure generates better precise position tracking and demonstrates more favourable stability.

This paper can be further improved in several directions. For example, it is necessary to build a stable organizing method [33, 34] to reduce the node number's instability. In addition, it is also crucial to apply our system to control real-time models and to deal with the chattering problems in real dynamic systems.

A. Appendix

The Lyapunov function is used to analyze the asymptotic stability of the control system based on the proposed T2WBD. The Lyapunov function of the proposed controller is defined as:

$$\begin{aligned} V = & \frac{1}{2}s^T s + \frac{1}{2}\operatorname{tr}\left(\tilde{\tilde{w}}^T \eta_1 \tilde{\tilde{w}}\right) + \frac{1}{2}\operatorname{tr}\left(\tilde{\mu}^T \eta_3 \tilde{\mu}\right) + \frac{1}{2}\operatorname{tr}\left(\tilde{\tilde{\sigma}}^T \eta_4 \tilde{\tilde{\sigma}}\right) \\ & + \frac{1}{2}\operatorname{tr}\left(\underline{\tilde{\sigma}}^T \eta_5 \underline{\tilde{\sigma}}\right) + \frac{1}{2}\operatorname{tr}\left(\iota\tilde{\tilde{w}} r^T \eta_6 \iota\tilde{\tilde{w}} r\right) + \frac{1}{2}\operatorname{tr}\left(\underline{\iota\tilde{w}} r^T \eta_7 \underline{\iota\tilde{w}} r\right) \\ & + \frac{1}{2}\operatorname{tr}\left(\tilde{\kappa}^T \eta_8 \tilde{\kappa}\right). \end{aligned} \tag{63}$$

The derivation on both sides of the equation is:

$$\begin{aligned} \dot{V} = & s^T \dot{s} + \operatorname{tr}\left(\tilde{\tilde{w}}^T \eta_1 \dot{\tilde{\tilde{w}}}\right) + \operatorname{tr}\left(\tilde{\mu}^T \eta_3 \dot{\tilde{\mu}}\right) + \operatorname{tr}\left(\dot{\tilde{\tilde{\sigma}}}^T \eta_4 \dot{\tilde{\tilde{\sigma}}}\right) + \\ & \operatorname{tr}\left(\underline{\tilde{\sigma}}^T \eta_5 \underline{\dot{\tilde{\sigma}}}\right) + \operatorname{tr}\left(\iota\tilde{\tilde{w}} r^T \eta_6 \iota\dot{\tilde{\tilde{w}}} r\right) + \operatorname{tr}\left(\underline{\iota\tilde{w}} r^T \eta_7 \underline{\iota\dot{w}} r\right) \\ & + \operatorname{tr}\left(\tilde{\kappa}^T \eta_8 \dot{\tilde{\kappa}}\right). \end{aligned} \tag{64}$$

Substitute Eqs. 37 and 54 into Eq. 64, we have:

$$\begin{aligned} \dot{V} = & s^T\{\lambda_1[\hat{\tilde{w}}(D\bar{F}_\mu \cdot \tilde{\mu} + D\bar{F}_{\tilde{\sigma}} \cdot \tilde{\tilde{\sigma}} + D\bar{F}_{\iota\bar{w}r} \cdot \tilde{\tilde{w}} r + D\bar{F}_\kappa \cdot \tilde{\kappa}) \\ & + \hat{\tilde{w}}(D\underline{F}_\mu \cdot \tilde{\mu} + D\underline{F}_{\underline{\sigma}} \cdot \tilde{\sigma} + D\underline{F}_{\underline{\iota w r}} \cdot \underline{\iota\tilde{w}} r + D\underline{F}_\kappa \cdot \tilde{\kappa}) \\ & + \tilde{\tilde{w}}\hat{\tilde{F}} + \tilde{\tilde{w}}\underline{\hat{F}}] + \lambda_1\tau - \lambda_1 F - U_{rc}\} \\ & + \operatorname{tr}(\tilde{\tilde{w}}^T \eta_1 \dot{\tilde{\tilde{w}}}) + \operatorname{tr}(\tilde{\mu}^T \eta_3 \dot{\tilde{\mu}}) + \operatorname{tr}(\tilde{\tilde{\sigma}}^T \eta_4 \dot{\tilde{\tilde{\sigma}}}) + \operatorname{tr}(\underline{\tilde{\sigma}}^T \eta_5 \underline{\dot{\tilde{\sigma}}}) \\ & + \operatorname{tr}(\iota\tilde{\tilde{w}} r^T \eta_6 \iota\dot{\tilde{\tilde{w}}} r) + \operatorname{tr}(\underline{\iota\tilde{w}} r^T \eta_7 \underline{\iota\dot{w}} r) + \operatorname{tr}(\tilde{\kappa}^T \eta_8 \dot{\tilde{\kappa}}). \end{aligned} \tag{65}$$

Therefore, set $s^T\lambda_1\tilde{\tilde{w}}\hat{\tilde{F}} + s^T\lambda_1\tilde{\tilde{w}}\underline{\hat{F}} + tr\left(\tilde{\tilde{w}}^T\eta_1\dot{\tilde{\tilde{w}}}\right) = 0$, we then have:

$$\dot{\tilde{\tilde{w}}} = -\frac{\hat{F}^T s^T \lambda_1}{\eta_1}. \tag{66}$$

Set $s^T\lambda_1\hat{\tilde{w}}D\overline{F}_\mu\tilde{\mu} + s^T\lambda_1\hat{\tilde{w}}D\underline{F}_\mu\tilde{\mu} + tr\left(\tilde{\mu}^T\eta_3\dot{\tilde{\mu}}\right) = 0$, the following holds:

$$\dot{\tilde{\mu}} = -\frac{s^T\lambda_1\hat{\tilde{w}}(D\overline{F}_\mu + D\underline{F}_\mu)}{\eta_3}. \tag{67}$$

Set $s^T \lambda_1 \hat{\omega} D\overline{F}_{\bar{\sigma}} \tilde{\bar{\sigma}} + tr\left(\tilde{\bar{\sigma}}^T \eta_4 \dot{\tilde{\bar{\sigma}}}\right) = 0$, then we have:

$$\dot{\tilde{\bar{\sigma}}} = -\frac{s^T \lambda_1 \hat{\omega} D\overline{F}_{\bar{\sigma}}}{\eta_4}. \tag{68}$$

Set $s^T \lambda_1 \hat{\omega} D\underline{F}_{\underline{\sigma}} \underline{\tilde{\sigma}} + tr\left(\underline{\tilde{\sigma}}^T \eta_5 \underline{\dot{\tilde{\sigma}}}\right) = 0$, then we have:

$$\underline{\dot{\tilde{\sigma}}} = -\frac{s^T \lambda_1 \hat{\omega} D\underline{F}_{\underline{\sigma}}}{\eta_5}. \tag{69}$$

Set $s^T \lambda_1 \hat{\omega} D\overline{F}_{\omega\bar{r}} \omega\tilde{\bar{r}} + tr\left(\omega\tilde{\bar{r}}^T \eta_6 \omega\dot{\tilde{\bar{r}}}\right) = 0$, then we have:

$$\omega\dot{\tilde{\bar{r}}} = -\frac{s^T \lambda_1 \hat{\omega} D\overline{F}_{\omega\bar{r}}}{\eta_6} \tag{70}$$

Set $s^T \lambda_1 \hat{\omega} D\underline{F}_{\underline{\omega r}} \cdot \underline{\omega r} + tr\left(\underline{\omega r}^T \eta_7 \underline{\dot{\omega r}}\right) = 0$, then we have:

$$\underline{\dot{\omega r}} = -\frac{s^T \lambda_1 \hat{\omega} D\underline{F}_{\underline{\omega r}}}{\eta_7}. \tag{71}$$

Set $s^T \lambda_1 \hat{\omega} D(D\bar{F}_{\kappa} + D\underline{F}_{\underline{\kappa}})\tilde{\kappa} + tr\left(\tilde{\kappa}^T \eta_8 \ \dot{\tilde{\kappa}}\right) = 0$, then we have:

$$\dot{\tilde{\kappa}} = -\frac{s^T \lambda_1 \hat{\omega} D(D\bar{F}_{\kappa} + D\underline{F}_{\underline{\kappa}})}{\eta_8}. \tag{72}$$

Substitute Eqs. (66-72) into Eq. (65), we have:

$$\begin{aligned} \dot{V} &= s^T \left[\lambda_1 \tau - \lambda_1 F - U_{rc}\right] \\ &= s^T \left[\lambda_1 \tau - \lambda_1 F - \sigma sgn(s)\right] \\ &\leq -|s| \left[\sigma - \lambda_1 \tau_0 - \lambda_1 F_d\right]. \end{aligned} \tag{73}$$

The update rule of $\underline{w}$ is determined by the emotional update rule:

$$\underline{\dot{w}} = \alpha \cdot [\max(0, d - a) \cdot F], \tag{74}$$

where α is a learning rate, and d can be expressed as:

$$d = b \cdot ss + c \cdot nn. \tag{75}$$

where b and c are given parameters. In Eq. 73, σ is set to be slightly larger than $\lambda_1\left(F_d + \tau_0\right)$, that is, $\sigma \geq \lambda_1\left(F_d + \tau_0\right) + \xi$. Then $\dot{V} \leq -\xi\left|s^T\right| \leq 0$. Thus $\dot{V}$ is a semi-negative definite value, which means $\dot{V}$ is bounded.

From $\dot{V} \leq -\xi\left|s^T\right|$, we have:

$$\int_0^t \left|s^T\right| dt \leq (1/\xi)(V(0) - V(t)). \tag{76}$$

Because $V(0)$ is bounded, and $V(t)$ is bounded and non-incremental, $\int_0^t \left|s^T\right| dt$ is bounded. In addition, $\dot{s}$ is bounded. According to Barbalat's lemma, the following equation has been proved:

$$\lim_{t\to\infty} s = 0 \tag{77}$$

CRediT authorship contribution statement

Zi-Qi Wang: Methodology, Software. **Li-Jiang Li:** Methodology, Software. **Fei Chao:** Conceptualization of this study, Methodology, Investigation, Writing - Original draft preparation. **Chih-Min Lin:** Conceptualization of this study. **Longzhi Yang:** Writing - Review & Editing. **Changle Zhou:** Formal analysis. **Xiang Chang:** Data Curation, Investigation. **Changjing Shang:** Supervision. **Qiang Shen:** Supervision.

References

[1] Badar, R., Dilshad, S., 2020. Adaptive Type-2 neurofuzzy wavelet-based supplementary damping controls for statcom. International Transactions on Electrical Energy Systems 30.

[2] Cao, Y., Jiang, W., Wang, J., 2021. Anti-synchronization of delayed memristive neural networks with leakage term and reaction–diffusion terms. Knowledge-Based Systems 233, 107539. URL: https://www.sciencedirect.com/science/article/pii/S0950705121008017, doi:https://doi.org/10.1016/j.knosys.2021.107539.

[3] Chao, F., Zhou, D., Lin, C.M., Yang, L., Zhou, C., Shang, C., 2020. Type-2 fuzzy hybrid controller network for robotic systems. IEEE Transactions on Cybernetics 50, 3778–3792. doi:10.1109/TCYB.2019.2919128.

[4] Cheng, L., Hou, Z., Lin, Y., Tan, M., Zhang, W.C., Wu, F., 2011. Recurrent neural network for non-smooth convex optimization problems with application to the identification of genetic regulatory networks. IEEE Transactions on Neural Networks 22, 714–726.

[5] Chu, Y., Fei, J., Hou, S., 2020. Adaptive global sliding-mode control for dynamic systems using double hidden layer recurrent neural network structure. IEEE Transactions on Neural Networks and Learning Systems 31, 1297–1309.

[6] Fang, W., Chao, F., Lin, C.M., Yang, L., Shang, C., Zhou, C., 2019. An improved fuzzy brain emotional learning model network controller for humanoid robots. Frontiers in Neurorobotics 13. URL: https://www.frontiersin.org/article/10.3389/fnbot.2019.00002, doi:10.3389/fnbot.2019.00002.

[7] Fang, W., Chao, F., Lin, C.M., Zhou, D., Yang, L., Chang, X., Shen, Q., Shang, C., 2021. Visual-guided robotic object grasping using dual neural network controllers. IEEE Transactions on Industrial Informatics 17, 2282–2291. doi:10.1109/TII.2020.2995142.

[8] Fei, J., Chen, Y., 2020. Dynamic terminal sliding-mode control for single-phase active power filter using new feedback recurrent neural network. IEEE Transactions on Power Electronics 35, 9906–9924.

[9] Fei, J., Fang, Y., Yuan, Z., 2020. Adaptive fuzzy sliding mode control for a micro gyroscope with backstepping controller. Micromachines 11.

[10] Fei, J., Feng, Z.L., 2021. Adaptive super-twisting sliding mode control for micro gyroscope based on double loop fuzzy neural network structure. International Journal of Machine Learning and Cybernetics 12, 611–624.

[11] Fei, J., Lu, C., 2018. Adaptive sliding mode control of dynamic systems using double loop recurrent neural network structure. IEEE Transactions on Neural Networks and Learning Systems 29, 1275–1286.

[12] Gao, S., Zhao, D.Y., Yan, X., Spurgeon, S., 2020. Linearized bregman iteration based model-free adaptive sliding mode control for a class of non-linear systems. IET Control Theory and Applications .

[13] Guan, X., Hu, J., Qi, J., Chen, D., Zhang, F., Yang, G., 2021. Observer-based hsliding mode control for networked systems subject to communication channel fading and randomly varying nonlinearities. Neurocomputing 437, 312–324.

[14] He, S., Xu, Y., Wu, Y., Li, Y., Zhong, W., 2021. Adaptive consensus tracking of multi-robotic systems via using integral sliding mode control. Neurocomputing .

[15] Hsu, C.F., Chen, B.R., Wu, B.F., 2022. Broad-learning recurrent hermite neural control for unknown nonlinear systems. Knowledge-Based Systems 242, 108263. URL: https://www.sciencedirect.com/science/article/pii/S0950705122000831, doi:https://doi.org/10.1016/j.knosys.2022.108263.

[16] Huynh, T., Lin, C., Le, T., Zhong, Z., 2020a. A mixed gaussian membership function fuzzy CMAC for a three-link robot, in: 29th IEEE International Conference on Fuzzy Systems, FUZZ-IEEE 2020, Glasgow, UK, July 19-24, 2020, IEEE. pp. 1–7.

[17] Huynh, T.T., Lin, C.M., Le, T.L., Nguyen, N.P., Hong, S., Chao, F., 2020b. Wavelet interval Type-2 fuzzy quad-function-link brain emotional control algorithm for the synchronization of 3d nonlinear chaotic systems. International Journal of Fuzzy Systems 22, 2546–2564.

[18] Junejo, A.K., Xu, W., Mu, C., Ismail, M.M., Liu, Y., 2020. Adaptive speed control of pmsm drive system based a new sliding-mode reaching law. IEEE Transactions on Power Electronics 35, 12110–12121.

[19] Le, T.L., Huynh, T.T., Lin, C.M., 2019. Self-evolving interval Type-2 wavelet cerebellar model articulation control design for uncertain nonlinear systems using pso. International Journal of Fuzzy Systems 21, 2524–2541.

[20] Lin, C., Chung, C.C., 2015. Fuzzy brain emotional learning control system design for nonlinear systems. International Journal of Fuzzy Systems 17, 117–128.

[21] Lin, C.M., La, V.H., Le, T.L., 2018. Dc–dc converters design using a Type-2 wavelet fuzzy cerebellar model articulation controller. Neural Computing and Applications 32, 2217–2229.

[22] Ma, B., Li, Y., An, T., Dong, B., 2021. Compensator-critic structure-based neuro-optimal control of modular robot manipulators with uncertain environmental contacts using non-zero-sum games. Knowledge-Based Systems 224, 107100. URL: https://www.sciencedirect.com/science/article/pii/S0950705121003634, doi:https://doi.org/10.1016/j.knosys.2021.107100.

[23] Mohammadzadeh, A., Zhang, W., 2019. Dynamic programming strategy based on a type-2 fuzzy wavelet neural network. Nonlinear Dynamics 95, 1661–1672.

[24] Ni, J., Ahn, C., Liu, L., xin Liu, C., 2019. Prescribed performance fixed-time recurrent neural network control for uncertain nonlinear systems. Neurocomputing 363, 351–365.

[25] Ren, Y., Zhou, W., Li, Z., Liu, L., Sun, Y., 2021. Prescribed-time leader-following consensus for stochastic second-order multi-agent systems subject to actuator failures via sliding mode control strategy. Neurocomputing 425, 82–95.

[26] Tafti, B.E.F., Teshnehlab, M., Khanesar, M.A., 2020. Recurrent interval type-2 fuzzy wavelet neural network with stable learning algorithm: Application to model-based predictive control. International Journal of Fuzzy Systems 22, 351–367.

[27] Wang, L., Zeng, K., Hu, C., Zhou, Y., 2022. Multiple finite-time synchronization of delayed inertial neural networks via a unified control scheme. Knowledge-Based Systems 236, 107785. URL: https://www.sciencedirect.com/science/article/pii/S0950705121009977, doi:https://doi.org/10.1016/j.knosys.2021.107785.

[28] Wang, W., Jia, X., Wang, Z., Luo, X., Li, L., Kurths, J., Yuan, M., 2020a. Fixed-time synchronization of fractional order memristive mam neural networks by sliding mode control. Neurocomputing 401, 364–376.

[29] Wang, Y., Sun, J., He, H., Sun, C., 2020b. Deterministic policy gradient with integral compensator for robust quadrotor control. IEEE Transactions on Systems, Man, and Cybernetics: Systems 50, 3713–3725.

[30] Xiao, J., Li, Y., Wen, S., 2021. Mittag-leffler synchronization and stability analysis for neural networks in the fractional-order multi-dimension field. Knowledge-Based Systems 231, 107404. URL: https://www.sciencedirect.com/science/article/pii/S0950705121006663, doi:https://doi.org/10.1016/j.knosys.2021.107404.

[31] Xie, Z., Sun, T., Kwan, T., Wu, X., 2020. Motion control of a space manipulator using fuzzy sliding mode control with reinforcement learning. Acta Astronautica 176, 156–172.

[32] Yue, Y., Yang, H., Liu, F., Zang, H., 2021. Cooperative control for multiple quadrotors under position deviations and aerodynamic drag. Mechanical Systems and Signal Processing 147, 107096.

[33] Zhang, H., Hu, B., Wang, X., Xu, J., Wang, L., Sun, Q., Wang, Z., 2021. Self-organizing deep belief modular echo state network for time series prediction. Knowledge-Based Systems 222, 107007. URL: https://www.sciencedirect.com/science/article/pii/S0950705121002707, doi:https://doi.org/10.1016/j.knosys.2021.107007.

[34] Zhang, J., Li, Q., Chang, X., Chao, F., Lin, C.M., Yang, L., Huynh, T.T., Zheng, L., Zhou, C., Shang, C., 2020. A novel self-organizing emotional cmac network for robotic control, in: 2020 International Joint Conference on Neural Networks (IJCNN), pp. 1–6. doi:10.1109/IJCNN48605.2020.9207710.

[35] Zhao, T., Liu, J., Dian, S., Guo, R., Li, S., 2020. Sliding-mode-control-theory-based adaptive general type-2 fuzzy neural network control for power-line inspection robots. Neurocomputing 401, 281–294.